# Chapter 17

# ISOTOPIC EFFECT ON THE LATTICE CONSTANT OF GERMANIUM AND SILICON

Alexander Kazimirov
*Cornell High Energy Synchrotron Source (CHESS),*
*Cornell University, Ithaca, NY 14853, USA*

Jörg Zegenhagen
*European Synchrotron Radiation Facility (ESRF),*
*BP 220, F-39043, Grenoble, France*

Evgeny Sozontov
*Institute of Crystallography (Kaluga Branch),*
*RAS, Akademicheskaya 8, Kaluga, 248640, Russia*

Victor Kohn
*Russian Research Center "Kurchatov Institute",*
*123182, Moscow, Russia*

Manuel Cardona
*Max-Planck-Institut für Festkörperforschung,*
*Heisenbergstr. 1, 70569 Stuttgart, Germany*

Angular dependences of intensity of photoelectron or fluorescence yield excited by the XSW field from the topmost layer of a sufficiently thick epitaxial film are extremely sensitive to the lattice constant difference between substrate and the film. This sensitivity has been used to study the influence of the isotopic mass on the lattice constant of Ge and Si. The samples were homoepitaxial films on a substrate with different isotopic composition. For samples of moderate crystalline quality the measurements were performed at the near backscattering geometry. This approach requires only miniscule amounts of isotopic pure materials and can be applied to materials that cannot be grown as high-quality single crystals.

## 17.1. Introduction

Crystals of the same chemical composition but built from different isotopes exhibit different lattice constants. This phenomenon is due to the effect of nuclear mass on the zero-point vibrations and the related anharmonicity of interatomic potentials. The effect is largest at low temperature, when the total energy is dominated by the zero-point motion, and vanishes when approaching the Debye temperature. It is stronger for lighter isotopes due to the higher zero-point energy. The lattice constant of a crystal consisting of the heavier isotope is smaller than that built from the lighter one. London, in one of the first theoretical papers on the subject,[1] explained this fact in the following way. Suppose we replaced the atoms in the crystal by their lighter isotope, then their vibration frequency, $\nu \sim \frac{1}{\sqrt{m}}$ for monatomic solids, will be higher. This will also usually happen when the temperature of the crystal is increased. This consideration clearly emphasizes the intrinsic relation of the isotopic effect to crystal thermal expansion (anharmonicity).

The interest in this effect has its origin in the 1930s in the discussions on the condensation of liquid He[2,3] a phenomenon in which the zero-point energy plays a critical role. Substituting isotopes in a crystal lattice was considered to be a straightforward way to change the total energy of crystal without changing its potential energy. The first measurements were performed for the lattice parameters of ordinary and "heavy" ice by using the oscillation technique[4] and for LiH and LiD by using powder diffraction,[5] followed by experiments on $^{6}$Li and $^{7}$Li fluorides[6] and metallic *Li*.[7] Ten years later, experiments on oxides $^{24}$MgO and $^{26}$MgO, $^{40}$CaO, and $^{48}$CaO, and $^{58}$NiO and $^{64}$NiO were performed at room and liquid $N_2$ temperatures.[8] Comparison of the experimental data published at that time revealed a remarkable difference of the isotopic effect between crystal with either van der Waals or ionic bonding. Measurements on lithium hydrides by using powder diffraction were reported later for a wide temperature range.[9] Improvement in accuracy of X-ray diffraction techniques led to precise measurements of the lattice constant difference of single crystal natural Ge and isotopically enriched $^{74}$Ge at room and liquid nitrogen temperatures by using a double-beam triple-axis spectrometer.[10] Measurements on synthetic single crystal diamond in the range of composition from $^{12}$C to $^{13}$C were performed in Refs. 11 and 12 by using high resolution diffractometry.

The sparseness of experimental data available was mainly due to the very limited amount of pure isotopes available to grow isotopically enriched crystals. At the beginning of our project in 1995 the situation drastically changed: large amounts of isotopic pure elements had become available in Russia as part of the "swords into plowshares" program stimulating comprehensive studies of the influence of the isotopic composition on basic physical properties of crystals such as thermal conductivity, phonon frequencies and line widths, selfdiffusion and others (for reviews, see e.g. Refs. 13–17).

Our original approach to study isotopic effects on lattice constant was to measure the lattice constant difference between a single crystal substrate and an epitaxial layer of different isotopic composition by using high-resolution X-ray diffraction. The advantages of this approach are a perfect alignment of the substrate and the film crystal lattices and also an additional enhancement of the *d*-spacing difference of the pseudomorphically grown (as a result of a negligible lattice constant mismatch at the growth temperature) film due to tetragonal elastic distortion normal to the surface. Estimations for Si showed that the separation of the diffraction peaks from a $^{nat}$Si substrate and a $^{30}$Si isotopically enriched film of reasonable thickness could be clearly observed and reliably measured by using high order reflections. Unfortunately, chemically pure Si isotopes were not available by that time and chemical impurities would have a much larger influence on the lattice constant than the isotopic composition. High purity germanium and Ge crystals were available, but the effect is considerably weaker for Ge and thus it required a much more sensitive technique.

## 17.2. Application of XSW for Precise Relative Lattice Constant Measurements

The development of the technique goes back to the pioneer work of Andersen *et al.*,[18] who measured the lattice relaxation caused by nitrogen implantation in Si by measuring the XSW fluorescent yield from arsenic atoms implanted in a very shallow surface layer. Recording the signal from the topmost layer is crucial for this method. The escape depth for photoelectrons is very small, typically a few tens of nanometers.[19] This offers specific advantages when using electrons instead of fluorescence,

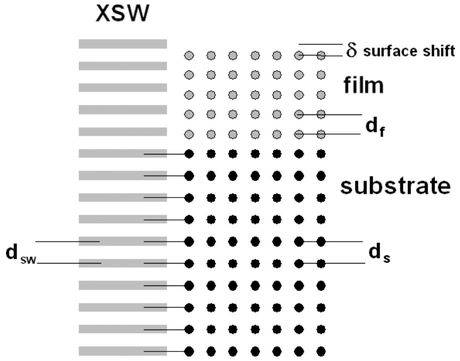

Fig. 17.1. Schematics of measuring small lattice mismatch by using standing waves. The $d$-spacing of the substrate lattice (black atoms) $d_s$ is slightly larger than the $d$-spacing $d_f$ of the epitaxial film (grey atoms). The standing wave shown on the left is generated by the diffraction from the substrate and has a periodicity of $d_{sw} = d_s$. Accumulated over the thickness of the film $d$-spacing difference results in a shift of the topmost layer by $\delta = (\Delta d/d)t_f$, where $t_f$ is the thickness of the film.

leading to the development of the XSW techniques based on measuring the photoelectron yield either in vacuum[20] or by using a gas flow proportional counter.[21] The method has been successfully applied to study strain gradients in epitaxial Ge and GaAs bicrystal structures[22] and small deformations in thin Si epitaxial films.[23]

The basics of the technique are illustrated in Fig. 17.1. Consider an epitaxial film with the $d$-spacing $d_f$ slightly smaller than the $d$-spacing $d_s$ of the substrate. As a result of the lattice mismatch $\Delta d/d = (d_f - d_s)/d_s$ the topmost layer of the film is now displaced by the amount of $\delta = (\Delta d/d)t_f$ accumulated over the thickness of the film with respect to the position in the case of the zero mismatch $d_f = d_s$. The standing wave is generated by the diffraction from the bulk of the substrate and therefore it has the period $d_{sw} = d_s$ of the substrate $d$-spacing for the chosen reflection. If the signal, either fluorescence or photoelectrons, from the atoms of the topmost atomic layer is recorded then the XSW yield curves (the coherent position $P^H$) acquires an additional phase shift of $\Delta\varphi = 2\pi P^H = 2\pi(\delta/d_{sw})$. For the standing wave to have the period of $d_{sw}$ determined mostly by the substrate, the extinction length $L_{ex}$ for the chosen reflection must be larger than the thickness of the film, which usually requires the use of high-order reflections. The second important condition determining the sensitivity to the surface displacement requires that the yield depth of the secondary radiation must be much smaller than the thickness of the film $L_{yi} \ll t_f$.

In the ideal case of $L_{yi} \ll t_f \ll L_{ex}$, the XSW data can be treated by using the standard XSW yield equation for perfect crystals (*cf.* Chapter 1). For real samples, the effect of the layer on the local phase of the XSW field cannot be neglected and the theory of the XSW in layered crystals developed in Refs. 24–28 and presented in Chapter 3, is needed for the accurate data analysis.

## 17.3. Experiment

Samples with isotopically highly enriched epitaxial films have been grown at the MPI-FKF institute in Stuttgart by using molecular beam epitaxy (Ge) and liquid phase epitaxy (Si). Since the total surface shift is proportional to the thickness of the film, special care has been taken for accurate calibration of the growth rate. The final thickness has been measured by using SIMS and AFM techniques. The XSW measurements have been performed over a wide temperature range by using a laboratory X-ray setup ($^{nat}$Ge/$^{76}$Ge) at the MPI-FKF and the RÖMO beamline at HASYLAB (*cf.* Appendix 5 by G. Materlik).

### 17.3.1. *Lattice constant measurements for germanium: $^{nat}$Ge/$^{76}$Ge and $^{70}$Ge/$^{76}$Ge*

The samples were grown in an MBE system with a base pressure below $10^{-10}$ mbar. The Ge(111) substrate was prepared in UHV by degassing and sputter-annealing to produce a sharp $c(2 \times 8)$ reconstruction. The cleanliness of the surface was controlled by Auger electron spectroscopy. The source material, about 100 mg of $^{76}$Ge, was kept at 1450°C in the Knudsen cell, equipped with a liquid nitrogen shroud, leading to a constant growth rate of 0.92 nm/min during the total deposition time of about 25 h. In order to obtain a smooth Ge film, the substrate temperature was slowly ramped from 250°C to 500°C during the first minutes of growth. To ensure the absence of any residual impurities in the film, the whole MBE chamber had been carefully cleaned before the start of the project. As a proof of cleanliness, we obtained a zero-phase shift in the XSW yield for a $^{nat}$Ge/$^{nat}$Ge control samples prepared under the same conditions. Two samples were grown: (1) an isotopically enriched $^{76}$Ge film with a thickness of $1.36 \pm 0.01\,\mu$m and an average isotope mass of $\overline{M} = 75.72$ on a perfect $^{nat}$Ge (111) substrate resulting in a mass difference of $\Delta M = 3.05$, and (2) an isotopically enriched $^{76}$Ge film with a thickness of $0.56 \pm 0.01\,\mu$m and

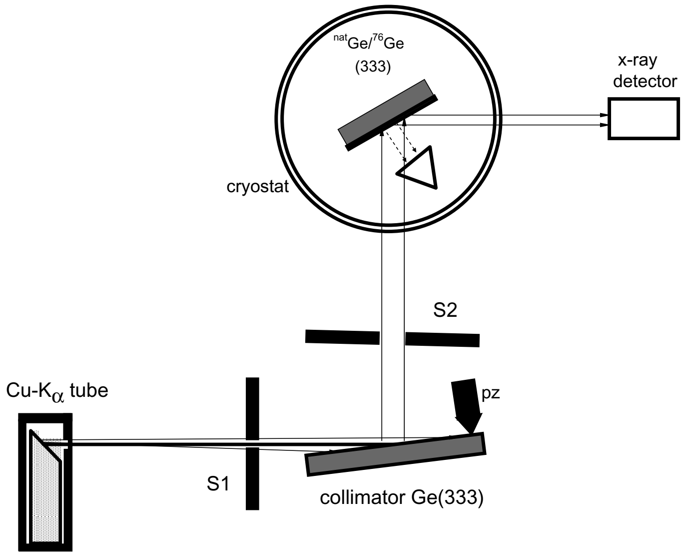

Fig. 17.2. Laboratory XSW setup. The X-ray beam is collimated by an asymmetrical monochromator crystal. The sample is mounted inside a He-flow-through cryostat. The photoelectron yield is measured by a channeltron and the diffracted beam is monitored by the scintillation detector. Angular scans are performed by scanning the collimator crystals by using a piezocrystal.

the same isotopic composition as for the sample #1, but grown on a single crystal $^{70}$Ge(111) substrate with the average isotope mass of $\overline{M} = 70.08$.

Sample #1 was measured by using a home-made laboratory setup based on a double-crystal diffractometer, as shown in Fig. 17.2. The Cu-K$_\alpha$ radiation from a 1.5 kW generator, collimated by an asymmetrical Ge(333) crystal (*cf.* Chapter 13), was incident on the sample mounted inside a He flow-through cryostat. The XSW measurements were performed by scanning the collimator crystal with the help of a piezocrystal. The photoelectrons from the sample, excited by the XSW field, were collected by a channeltron at a grazing angle of 0° to 15° to further reduce the escape depth. The photoelectron yield curves for different temperatures and the Ge(333) rocking curve are shown in Fig. 17.3. The phase change by about $\pi$ is clearly observed while cooling the sample from room temperature to 54 K, which corresponds to a shift of the crystal surface inward by about $d_{333}^{Ge}/2 = 54.4$ pm. The experimental curves were fitted with the XSW theory for multilayer crystals[27] (*cf.* Chapter 3) by using the lattice constant mismatch (difference in Bragg angles of the substrate and the layer) as a

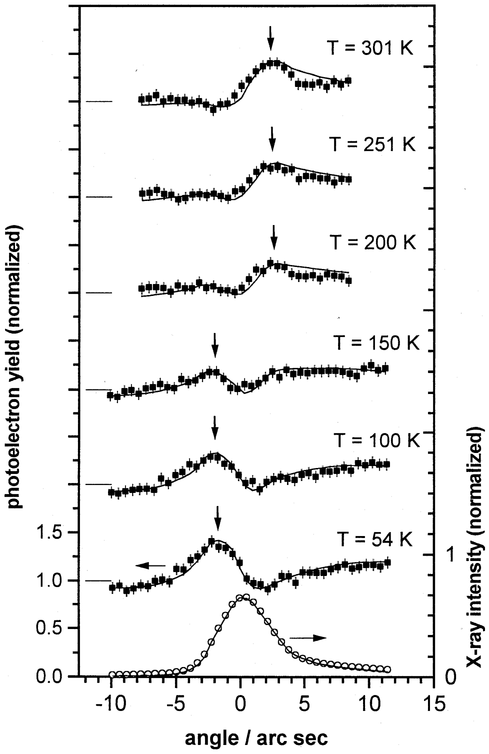

Fig. 17.3. Photoelectron Ge(333) XSW yield curves measured from the ${}^{nat}$Ge/${}^{76}$Ge sample at different temperatures. Ge(333) rocking curve is shown at the bottom. The phase shift $\Delta\varphi \approx \pi$ is clearly observed while cooling the sample from 300 K to 54 K (from Ref. 28).

fitting parameter. Because of the tetragonal distortion, the values obtained from the fit were then converted to relative lattice constant difference based on the well known elastic constants for Ge. The results scaled to $\Delta M = 1$ are displayed in Fig. 17.4 by the blue solid circles.[28]

The ${}^{70}$Ge single crystal, which served as a substrate for the sample #2, was grown by the Bridgman technique and initially showed excellent X-ray rocking curves, very close to the theoretical ones. However, because of various technical difficulties, it needed three attempts to finally grow the ${}^{76}$Ge epitaxial layer of appropriate thickness. As a result, because of the thermal treatment and/or the subsequently needed re-polishing, the crystalline quality deteriorated and the sample showed finally a mosaic spread of about 0.3 degree, making it unsuitable for the standard XSW

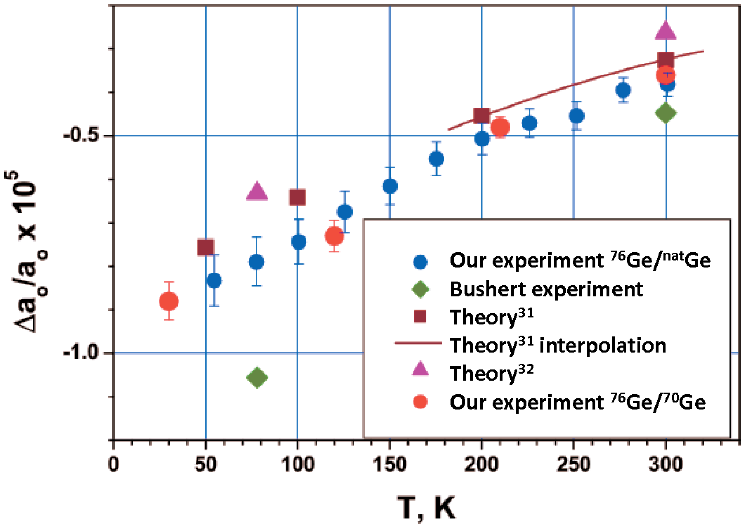

Fig. 17.4. Experimental results from two *Ge* samples scaled to $\Delta M = 1$. For comparison the results from the earlier experiment and from theory are also shown.

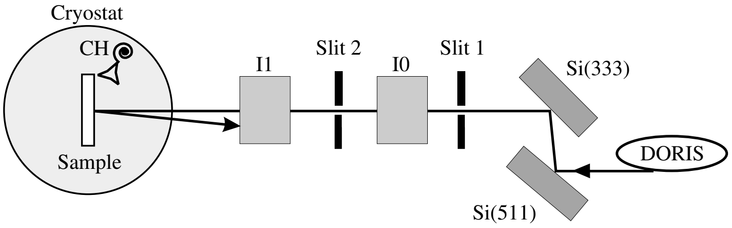

Fig. 17.5. Experimental set-up at the RÖMO beamline at HASYLAB. The X-ray beam is monochromatized by the double-crystal Si(511)/Si(333) monochromator with the energy bandpass of 0.3 eV. The energy of 7.59 keV corresponds to the near backscattering condition for the Ge(444) reflection from the sample. Two ionization chambers (I0, I1) measure the beam intensity. Electrons from the sample are detected by a channeltron (CH) (from Ref. 32).

technique. Thus, the sample was measured in the near backscattering geometry[29] which is known to be much less sensitive to mosaicity[30,31] (see Chapter 4). The experimental setup at the RÖMO beamline at HASYLAB is shown in Fig. 17.5.

A double-crystal Si(511)/Si(333) monochromator was used to produce the X-ray incident beam with an energy bandpass of 0.3 eV at an energy around 7.59 keV. The photoelectron yield curves were collected at different

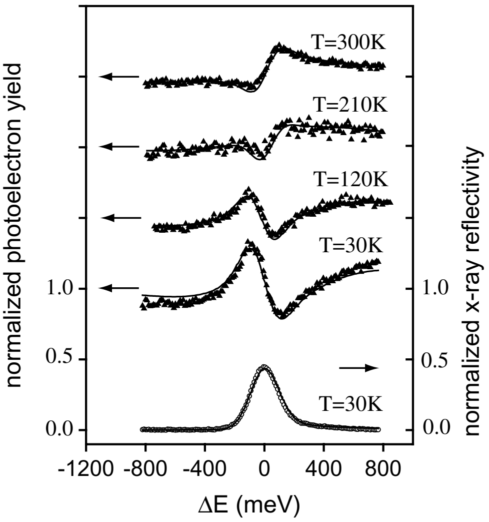

Fig. 17.6. Experimental photoelectron XSW yield curves from the $^{70}$Ge/$^{76}$Ge sample measured at near backscattering condition, Ge(444) reflection (from Ref. 32).

temperatures by scanning the energy of the beam through the Ge(444) reflection.[32] As one can see from Fig. 17.6, the angular positions of maximum and minimum of the XSW yield change when cooling the sample from 300 K to 30 K due to the shift of the surface layers by about $d_{444}^{Ge}/2 = 40.8\,\text{pm}$.

The experimental values of the isotopic effect scaled to $\Delta M = 1$ for the sample #2 are shown in Fig. 17.4 as red solid circles. In the same graph experimental data from the earlier work[10] are shown along with calculations based on density-functional perturbation theory[33] and path-integral Monte-Carlo simulations.[34]

### 17.3.2. *Lattice constant measurement for silicon: $^{nat}$Si/$^{30}$Si*

A few years after the start of our project chemically pure silicon isotopes became available in sufficient quantities. An isotopically enriched $^{30}$Si film (60% $^{30}$Si, 40% $^{28}$Si, $M = 29.20$) with a thickness of $0.92\,\mu$m was grown on a perfect single crystal Si(111) substrate with natural isotopic composition (91% $^{28}$Si, 4% $^{29}$Si, 5% $^{30}$Si, $M = 28.14$) by liquid phase epitaxy. The measurements were performed by using the laboratory setup discussed above (*cf.* Fig. 17.2. Experimental data scaled to $\Delta M = 1$ are shown in Fig. 17.7 together with theoretical calculations.[36,37] Note the

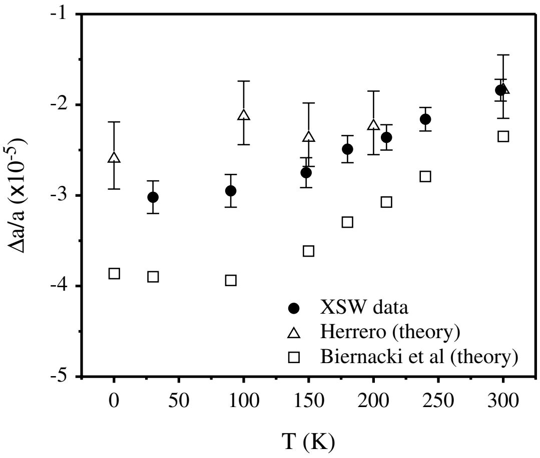

Fig. 17.7. First experimental data (solid circles) from the ${}^{nat}$Si/${}^{30}$Si sample measured by using laboratory XSW setup and scaled to $\Delta M = 1$. Results from theory are shown by open triangles[35] and open squares[36] (from Ref. 32).

much stronger effect for lighter Si than for Ge: Fig. 17.7 yields for $T \approx 0\,\mathrm{K}$ $\Delta a_0/a_0 \approx -3\times10^{-5}$ whereas in Fig. 17.4 we read $\Delta a_0/a_0 \approx -1\times10^{-5}$. It is easy to show[17] that the isotope effect in $\Delta a_0/a_0$ (normalized to $\Delta M = 1$) is proportional to $M^{-3/2}$. The ratio of the $-3/2$ power of the mass of silicon to that of germanium is 3.5, in rather good agreement with the corresponding isotope effects. This scaling law also applies to the corresponding isotope effect measured for diamond: $1.5 \times 10^{-4}$ for $\Delta M = 1$.[11] The ratio of this effect to that of germanium is 15 whereas $(M_C/M_{Ge})^{-3/2} = 14.3$. Later, high-resolution diffraction measurements at near backscattering conditions on a sample with the same isotopic composition but a film thickness of $15\,\mu$m were performed using high-order reflections.[37] The results agreed perfectly with our XSW data and revealed anomalous temperature behavior with the maximum of the isotopic effect at about $T = 75\,\mathrm{K}$ related to the negative expansion coefficient of silicon found below $110\,\mathrm{K}$.[38]

## 17.4. Conclusions

The XSW technique has been successfully applied to measure the isotopic effect on the lattice constant of Ge and Si crystals. Our approach requires only miniscule amounts of isotopic pure materials and moderate crystalline quality and it can be used to study materials that cannot be grown as high quality single crystals. We believe this technique can be applied to study other physical effects such as thermal expansion and related crystal dynamical properties of synthesized and engineerly tailored materials and may have technological applications in modern microelectronics and optoelectronics technology.

To estimate the limitation of the technique we consider as a simple example a Si crystal, X-rays with $\lambda = 70\,\text{pm}$ and a (555) reflection with the extinction length of $L_{ex} = 28\,\mu\text{m}$. An epitaxial film with the thickness of, say, $t = 6\,\mu\text{m}$ will still satisfies the condition that the XSW field is formed mostly by the substrate, $t \ll L_{ex}$. Then, the phase shift of $\pi$ will correspond to a lattice mismatch of $\Delta d/d \simeq 5\times 10^{-5}$. Taking a conservative value of 5% of $\pi$ as a detection limit, we can easily see that the relative lattice constant difference in the $10^{-7}$ range is well within the limits of this technique.

We conclude by noting that the isotope effect discussed here is also of interest in connection with an ongoing attempt to replace the present platinum-rhodium kilogram standard by an atomic standard based on the atomic mass of isotopic pure $^{28}$Si.[39,40] Finally, it should be noted that experimental data on the isotopic effect on lattice constants of crystals represent also a stringent, benchmark test for modern theoretical tools in solid state physics such as first-principal calculations.

## References

1. H. London, *Z. Physik. Chem.* **16** (1958) 302.
2. F. London, *Proc. Roy. Soc. A* **153** (1936) 576.
3. F. London, *J. Phys. Chem.* **43** (1939) 49.
4. H. D. Megaw, *Nature* **134** (1934) 900.
5. E. Zintle and A. Harder, *Z. Phys. Chem. B* **27–28** (1935) 478.
6. J. Thewlis, *Acta. Cryst.* **8** (1955) 36.
7. E. J. Covington and D. J. Montgomery, *J. Chem. Phys.* **27** (1957) 49.
8. V. S. Kogan and T. G. Omarov, *Sov. Phys. JETP* **20** (1965) 527.
9. J. L. Anderson, J. Nasise, K. Philipson and F. E. Pretzel, *J. Phys. Chem. Sol.* **31** (1970) 613.
10. R. C. Buschert, A. E. Merlini, S. Pace, S. Rodriguez and M. H. Grimsditch, *Phys. Rev. B* **38** (1988) 5219.
11. H. Holloway, K. C. Hass, M. A. Tamor, T. R. Anthony and W. F. Banholzer, *Phys. Rev. B* **44** (1991) 7123.
12. T. Yamanaka, S. Morimoto and H. Kanda, *Phys. Rev. B* **49** (1994) 9341.
13. M. Cardona, in *Advances in Solid State Physics*, Vol. 34, R. Helbig, ed. (Vieweg, Braunschweig/Wiesbaden, Germany, 1994), pp. 35.
14. M. Cardona, *Phys. Status Solidi (B)* **220** (2000) 5.
15. V. G. Plekhanov, *Physics-Uspekhi* **46** (2003) 689.

16. E. E. Haller, *Solid State Commun.* **133** (2005) 693.
17. M. Cardona and M. L. W. Thewalt, *Rev. Mod. Phys.* **77** (2005) 1173.
18. S. K. Andersen, J. A. Golovchenko and G. Mair, *Phys. Rev. Lett.* **37** (1976) 1141.
19. M. V. Kovalchuk, D. Liljequist and V. G. Kohn, *Sov. Phys. Sol. State* **28** (1986) 1918.
20. S. Kikuta, T. Takahashi and T. Tuzi, *Phys. Lett. A* **50** (1975) 453.
21. N. Hertel, M. V. Kovalchuk, A. M. Afanasev and R. M. Imamov, *Phys. Lett. A* **75** (1980) 501.
22. E. A. Sozontov, M. V. Kruglov and B. G. Zakharov, *Phys. Status Solidi (A)* **66** (1981) 303.
23. M. V. Kovalchuk, V. G. Kohn, E. F. Lobanovich, *Sov. Phys. Sol. State* **27** (1985) 2034.
24. A. M. Afanasev and V. G. Kohn, *Zh. Eksp. Teor. Fiz.* **74** (1978) 300 (In Russian);
25. A. M. Afanasev and V. G. Kohn, *Sov. Phys. JETP* **47** (1978) 154.
26. V. G. Kohn and M. V. Kovalchuk, *Phys. Status Solidi (A)*, **64** (1981) 359.
27. V. G. Kohn, *Phys. Status Solidi (B)*, **231** (2002) 132.
28. A. Kazimirov, J. Zegenhagen and M. Cardona, *Science* **282** (1998) 930.
29. K.-G. Huang, W. M. Gibson and J. Zegenhagen, *Phys. Rev. B* **40** (1989) 4216.
30. K. Kohra and T. Matsushita, *Z. Naturforsch. A* **27** (1972) 484.
31. W. Graeff and G. Materlik, *Nucl. Instr. Meth. A* **195** (1982) 97.
32. E. Sozontov, L. X. Cao, A. Kazimirov, V. Kohn, M. Konuma, M. Cardona and J. Zegenhagen, *Phys. Rev. Lett.* **86** (2001) 5329.
33. P. Pavone and S. Baroni, *Solid State Comun.* **90** (1994) 295.
34. J. C. Noya, C. P. Herrero and R. Ramírez, *Phys. Rev. B* **56** (1997) 237.
35. C. P. Herrero, *Solid State Commun.* **110** (1999) 243.
36. S. Biernacki and M. Scheffler, *J. Phys. Condens. Mat.* **6** (1994) 4849.
37. H. -C. Wille, Yu. V. Shvyd'ko, E. Gerdau, M. Lerche, M. Lucht, H. D. Rüter and J. Zegenhagen, *Phys. Rev. Lett.* **89** (2002) 285901.
38. K. G Lyon, G. L. Salinger, C. A. Swenson, G. K. White, *J. Appl. Phys* **48** (1977) 865.
39. P. Becker, D. Schiel, H. J. Pohl *et al.*, *Meas. Sci. Tech.* **17** (2006) 81.
40. P. Becker, P. De Bievre, K. Fuji *et al.*, *Metrologia* **44** (2007) 1854.